Chemical Engineering Journal 468 (2023) 143673

Contents lists available at ScienceDirect

Chemical Engineering Journal

journal homepage: www.elsevier.com/locate/cej

In-depth insights on multi-ionic transport in Electrodialysis with bipolar membrane systems

Antonia Filingeri [a], Julio Lopez [a,b,c,*], Andrea Culcasi [a,*], Tamara Leon [b,c], Alessandro Tamburini [a,d], José Luis Cortina [b,c], Giorgio Micale [a], Andrea Cipollina [a]

[a] Dipartimento di Ingegneria, Università degli Studi di Palermo, viale delle Scienze ed. 6, 90128 Palermo, Italy
[b] Chemical Engineering Department, Escola d'Enginyeria de Barcelona Est (EEBE), Universitat Politècnica de Catalunya (UPC)-BarcelonaTECH, C/ Eduard Maristany 10-14, Campus Diagonal-Besòs, 08930 Barcelona, Spain
[c] Barcelona Research Center for Multiscale Science and Engineering, Campus Diagonal-Besòs, 08930 Barcelona, Spain
[d] ResourSEAs SrL, Viale delle Scienze, Ed.16, 90128 Palermo, Italy

ARTICLE INFO

Keywords:
Multi-ions
Transport numbers
Multi-component solution
Mixed electrolytes
membrane selectivity

ABSTRACT

Electrodialysis with Bipolar Membranes (EDBM) has become a key technology for valorising waste brine streams as a new chemical production route. Even though its application has been widely studied using single electrolyte solutions (e.g., NaCl or Na_2SO_4), there is still a lack of knowledge about using multi-ionic mixtures. For the first time, this work aims to evaluate the EDBM performance when treating synthetic solutions mimicking the waste brines produced in a integrated process for the valorisation of solar saltworks bitterns. The behaviour of a lab-scale EDBM unit was assessed using SUEZ ion exchange membranes (IEMs), operating at 300 A m^{-2}, and the ion transport through IEMs was investigated, based on the calculation of apparent transport numbers and selectivities.

The results highlighted that multi-ionic solutions barely affected the production of hydroxide ions. Chlorides were transported up to 7 times faster than sulphates across the anion-exchange membranes, while the cation-exchange membranes exhibited slightly higher selectivity for potassium than for sodium (~1.2). The current efficiencies ranged between 70 % and 80 %, while a minimum specific energy consumption of 1.60 kWh kg^{-1}_{NaOH} was obtained for the most concentrated brine at 1 mol L^{-1} OH^-.

These results provide novel and valuable information to support the development and implementation of EDBM as a sustainable technology for supporting a resource-efficient and competitive economy through on-site and delocalized chemicals production routes.

1. Introduction

In recent years, membrane technologies have attracted attention in the industry due to their ability to achieve comparable performance with conventional technologies, yet significantly reducing costs [1,2]. Over the past few decades, Electrodialysis (ED) has attracted the attention of both academic community and industries. ED is a membrane process adopting cation and anion exchange membranes (CEM and AEM, respectively) constituting channels separated by net spacers. Under the application of an electric field, anions tend to move towards the positive anode and cations towards the negative cathode, and the presence of selectively-charged membranes either inhibits or promotes their transport through them. Anions, for instance, are easily transported across the AEM, but their transport is hindered across the CEM, whereas the opposite occurs for cations. The result is the separation of the feed salt stream into diluted and concentrated solutions [3]. ED is a well-established method for seawater concentration for table salt production, for brackish water desalination and drinking water production [4,5], and considerable interest has been shown in its implementation for seawater desalination [6,7], although its application is still limited [8]. Recently, electro-membrane processes are gaining interest in their applications for the valorization of desalination brines, drinking water remineralization and process intensification [9–12], but also for treating

* Corresponding authors at: Chemical Engineering Department, Escola d'Enginyeria de Barcelona Est (EEBE), Universitat Politècnica de Catalunya (UPC)-BarcelonaTECH, C/ Eduard Maristany 10-14, Campus Diagonal-Besòs, 08930 Barcelona, Spain (J. Lopez); Dipartimento di Ingegneria, Università degli Studi di Palermo, viale delle Scienze ed. 6, 90128 Palermo, Italy (A. Culcasi).
E-mail addresses: julio.lopez.rodriguez@upc.edu (J. Lopez), andrea.culcasi@unipa.it (A. Culcasi).

https://doi.org/10.1016/j.cej.2023.143673
Received 2 March 2023; Received in revised form 21 April 2023; Accepted 19 May 2023
Available online 22 May 2023

List of abbreviations

Acronyms

AEM	Anion Exchange Membrane
BPM	Bipolar Membrane
CEM	Cation Exchange Membrane
DC	Direct Current
ED	Electrodialysis
EDBM	Electrodialysis with Bipolar Membranes
ERS	Electrode rinse solution
IEC	Ion Exchange Capacity [meq g^{-1} of resin]
IEM	Ion exchange membrane
SWRO	Seawater Reverse Osmosis

Symbols

CE	Current efficiency [%]
C	Solution concentration [mol L^{-1}]
F	Faraday constant [C mol^{-1}]
I	Current [A]
J	Ion flux [mol m^{-2} s^{-1}]
J_w	Water flux [mL m^{-2}·h^{-1}]
M	Molecular weight [g mol^{-1}]
N	Number of triplet
n	Produced moles [mol]
OCV	Open Circuit Voltage [V]
S	Active membrane surface [m^2]
SEC	Specific energy consumption [kWh kg^{-1}_{NaOH}]
Sel	Ion selectivity [-]
SP	Specific productivity [kg_{NaOH} m^{-2} y^{-1}]
t	Transport number [-]
U	Voltage [V]
V	Solution volume [L]
z	Ion valence

Greek symbols

τ	Time [s]

Subscripts and superscripts

Acid	Acid compartment
Ave	Average
Base	Base compartment
eo	Electro-osmotic
i	Ion
os	Osmotic
Pt	Platinum wires
ref	Reference ion
Salt	Salt
tot	Total
w	Water

organic streams, such as producing lactic acid [13], deacidification of cranberry juice [14] and and de-alcoholization of wine products [15].

Electrodialysis with Bipolar Membranes (EDBM) enables the conversion of an electrolyte stream into an acid and base streams [16]. A Bipolar Membrane (BPM) comprises a cation and an anion layer one on top of the other. Under the effect of an electric field, the water-dissociation reaction within the junction between the two BPM layers produces protons and hydroxide ions [17,18], while the passage of cations and anions of the salt solution through the CEM and AEM, present in the elementary unit constituting EDBM stacks, allows the generation of acidic or alkaline solutions. Worth noting that, in the presence of an electric field (10^9 V m^{-1} at the bipolar junction), the water

Table 1
Summary of EDBM applications for the production of acids and bases from brines.

Membrane	Solution composition	Experimental conditions	Acid and base concentrations	Impurities	Current Efficiency	Specific Energy Consumption	Ref.
Shan-dong Tian-wei (DF120) and He-bei Guang-ya Co. Lt. (BPM)	NaCl, 40 mS cm^{-1}	200 cm^2 20 V	0.9 mol L^{-1} HCl	–	47 %	6.25 kWh kg^{-1} HCl	[35]
PCCell (SK, PC Acid 60) and Fumatech (FBM)	76 g L^{-1} NaCl	64 cm^2 523 A m^{-2}	1.8 mol L^{-1} HCl 2 mol L^{-1} NaOH	Na (3.1 %) in the acid Cl (0.5 %) in the base	84 % (NaOH) 79 % (HCl)	n.d.	[36]
Ralex (CM-PP, AM-PP) and Fumatech (FBM)	58.5 g L^{-1} NaCl	100 cm^2 1000 A m^{-2} Volume ratio (salt to acid/base) 20:1	3.2 mol L^{-1} HCl 3.6 mol L^{-1} NaOH	–	–	41 kWh kg^{-1} HCl	[31]
SUEZ (AR103P, CR61P and AR103A-tr.)	117 g L^{-1} NaCl	280 cm^2 300 A m^{-2}	0.8 mol L^{-1} NaOH	–	78 % (NaOH)	2.3 kWh kg^{-1} NaOH	[30]
PCCell (PC-SK, PC Acid 60, and BM)	52 g L^{-1} NaCl	64 cm^2 410 A m^{-2}	0.90 mol L^{-1} HCl 0.66 mol L^{-1} NaOH	–	85.6 %	2.34 kWh kg^{-1} NaOH	[21]
PCCell (PC Acid 60, PC SK and PC BP)	200 g L^{-1} NaCl	64 cm^2 520 A m^{-2}	2.0 mol L^{-1} HCl 2.2 mol L^{-1} NaOH	–	–	2.23 kWh kg^{-1} NaOH	[37]
Astom (Neosepta CMB, AHA and BP-1)	25.8 g L^{-1}Na, 38.3 g L^{-1}Cl, 74 mg L^{-1} Mg,4.7 mg L^{-1} Ca, 76 mg L^{-1} SO_4, 896 mg L^{-1} K	55 cm^2 25 V Volume ratio salt/ acid/ base: 5:5:2	1.8 mol L^{-1} NaOH	K (0.14 %) and Cl (0.04 %) in the base	50 % (NaOH)	4.72 kWh kg^{-1} NaOH	[34]
Astom (Neosepta CMX, AMX and BP-1)	43 g L^{-1} Na_2SO_4 4.5 g L^{-1}Li	189 cm^2 300 A m^{-2} Volume ratio (salt to acid/base) 2:1	0.5 mol L^{-1} H_2SO_4 1.05 mol L^{-1} NaOH	Na (1.6 %) and Li (0.1 %) in the acid SO_4 (1.6 %) and Li (0.2 %) in the base	61 % (H_2SO_4)	1.45 kWh kg^{-1} Na_2SO_4	[38]
Astom (Neosepta CMB, ACM and BP-1E)	6.91 g L^{-1}Na, 0.14 g L^{-1} K, 10.6 g L^{-1}Cl, 43 mg L^{-1} HCO_3^-, 36 mg L^{-1} Br, 1.04 g L^{-1} SO_4	510 cm^2 25 V 3 cycles by replacing the brine	0.6 mol L^{-1} acid 0.7 mol L^{-1} base	SO_4 (7.7 %), Na (0.4 %), HCO_3^- (0.4 %) and Br (0.3 %) in the acid K (2.1 %) and Cl (0.6 %) in the base	66 % (NaOH)	1.81 kWh kg^{-1} NaOH	[33]

dissociation rate can be four to six orders of magnitude higher than in the absence of an electric field [19].

Given the above, EDBM can be used to valorize waste salt streams, enhancing the circularity within integrated treatment processes to produce on-site chemicals. For instance, EDBM has been proposed to be integrated within seawater reverse osmosis (SWRO) desalination plants, aiming to (i) diminish the discharge of the brine generated (ca. two times more concentrated than seawater) to the sea, thus reducing the impact in marine ecosystems [20–23], and (ii) produce valuable chemicals (e.g. HCl and NaOH). Another example of EDBM integration with other technologies is proposed in the SEArcularMINE European project [24], whose objective is the recovery of valuable elements from waste brines (bitterns) generated in seawater solar saltworks. Elements such as magnesium [25], lithium [26,27], and other trace elements [28] are recovered by following a fully circular approach [29]. In this case, EDBM becomes the core technology of the circularity approach, guaranteeing the on-site production of the required chemicals (i.e., acids and bases) from the exhausted brines generated along the process.

The potential production of acids and bases from brines using EDBM has been previously studied (see Table 1). When working with single-component NaCl solutions, authors reported the possibility of reaching concentrations up to 1 mol L^{-1} HCl and NaOH working at mild conditions (less than 300 A m^{-2}), showing Specific Energy Consumption (SEC) below 3 kWh kg^{-1} NaOH and Current Efficiencies (CE) higher than 75 % [30]. However, these achieved concentrations, far from the required commercial conditions, can be increased by working at higher current density or high feed to acid/salt volume ratios. As example, Herrero-González et al. [31] were able to reach concentrations of NaOH and HCl higher than 3 mol L^{-1}, working at 1000 A m^{-2} and salt to acid (and base) volume ratios of 20:1, implying SEC values of 41 kWh kg^{-1} HCl. When dealing with multi-component brines, one of the main concerns is the presence of Ca and Mg, which can cause scaling at the membrane surface. Different alternatives have been studied to avoid scaling, such as the use of nanofiltration and selective precipitation for polishing [21], mono-selective membranes [32] or selective precipitation [33]. Similarly to the case of NaCl solutions, concentrations below 1 mol L^{-1} acid and base were produced at low current densities, with SEC values ranging from 1.8 to 2.5 kWh kg^{-1} NaOH [21,33]. Higher concentrations of acid and bases have also been reported working at high volume ratios feed to acid/base. As example, Song et al. [34] reported concentrations of 1.8 mol L^{-1} NaOH working at volume ratios feed:acid:base of 5:5:2 at 25 V, with CE of 48 % and SEC and 4.85 kWh kg^{-1} NaOH. Even though the studies with multi-component solutions in the literature, the authors barely studied the transport of ions across the membranes, focusing only on the purities or the concentrations of other ions in the obtained products. For instance, Chen et al. [32] obtained acid and base purities of 99.99 % when working with mono-selective membranes, reporting the presence of Mg and Ca in the base (less than 2 mg L^{-1}), while SO_4^{2-} was found in the acid (14 mg L^{-1}). Similarly, Du et al. [33] when treating with Ca and Mg-free SWRO brine, reported base and acid purities of 91% and 97%, respectively. The main impurities in the acid were SO_4^{2-} (2.0 g L^{-1}), Na (117 mg L^{-1}), HCO_3^- (90 mg L^{-1}) and Br (82 mg L^{-1}), whereas the base contained K (345 mg L^{-1}) and Cl (101 mg L^{-1}).

It can be observed that EDBM technologies show interesting achievements to be implemented for industrial sustainability, as it allows to close the production loops by providing value to wastes [39]. However, certain limitations slow their implementation to an industrial scale, such as non-ideal perm-selectivity and electroosmosis [40].

As described above, most of the published works to the date only report the purities content of the acidic and alkaline streams, while few efforts were devoted to the description of the transport of competing ions. This study aims to fill this gap by studying the transport of ions in EDBM units when treating multi-component solutions for acid and base production. With this respect, experiments were performed with a laboratory-scale set-up from SUEZ (0.028 m^2) using SUEZ membranes at constant current density (300 A m^{-2}). The effect of brine composition (in terms of concentration and presence of other ions) on the EDBM performance was studied using synthetic multi-component solutions mimicking those coming from waste brines produced in seawater solar saltworks. Specifically, an effective methodology for the analysis of ion apparent transport numbers and selectivities was presented. Furthermore, other important figures of merit, such as SEC and CE were evaluated.

2. Materials and methods

The experimental campaign was conducted in an EDBM unit, equipped with SUEZ membranes and operating in closed-loop configuration to produce acidic and alkaline solutions from synthetic brines. Results obtained with multi-component solutions were compared with single NaCl solutions, to characterize ion transport phenomena and their influence on EDBM performance.

2.1. Materials and experimental set-up

The laboratory-scale EDBM unit (Electromat MkI ED STACK, supplied by SUEZ) was equipped with 5 triplets, with an active membrane area of 0.028 m^2. CR61N and AR103N were used as CEMs and AEMs while BPMs (CR61N-AR103N-tr) comprised cation (same as CEM) and anion (AEM-treated) layers, placed one on top of the other after wetting both layers and removing air bubbles between them. The anion layer used in the BPM differs from a common AEM as it contains a catalyst to enhance water dissociation reactions [41].

Table 2 reports the main membrane properties [42]. Polystyrene spacers of 760 μm thickness were interposed between the membranes to create the solution channels, while for the electrode rinse solution (ERS) compartment, two overlapped spacers were used to double the fluid volume in the cathodic and anodic channels. Cathode and anode were constituted by stainless steel plate and stainless steel with platinum coating plate, respectively. In order to monitor the voltage drop through the 5 triplets, excluding the voltage drop across the electrodic compartments from the overall applied voltage, platinum wires with a diameter of 127 μm (99.9 % metal basis, Alfa Aesar) were interposed between the cathodic spacer and first CEM and between the last CEM (used as end-membrane) and the anodic spacer during the stack assembly (see Fig. 1a).

The experimental campaign was conducted with synthetic solutions (detailed compositions are reported in Table 3) prepared with demineralized water and the addition of salts, namely: NaCl (greater than 99.5 % purity, Saline di Volterra s.r.L., Italy), Na_2SO_4 (technical grade, CR GRUPO CRIMIDESA), and KCl (≥ 99 % purity, SIGMA-ALDRICH). The acid and alkaline solutions were prepared with solid NaOH micropearls (technical grade, Inovyn) and a concentrated solution of HCl (ACS Reagent 37%, Honeywell, Fluka), respectively. A 0.25 mol L^{-1} Na_2SO_4 solution was recirculated in both the anodic and cathodic compartments as the ERS.

Fig. 1b shows a scheme of the experimental set-up. The hydraulic circuit volume was identical for all four compartments (acid, basic, salt and ERS). The solutions were fed into the stack using peristaltic pumps (YT15, BT601S Lead Fluid, CO LTD, China). Pressure gauges (Cewal) were installed to monitor pressure drops across each hydraulic circuit. The solution mass variation during the test was measured using precision scales (KERN KB, Max 10,000 g, d = 0.1 g). A DC power supply (1902B, B&K precision) was utilized to generate the applied voltage at the electrodes, while two multimeters (Fluke 175) were connected, one in series and the other in parallel with the EDBM unit, to measure the electric current and voltage, respectively. The time-evolution of the electric conductivity and pH of the solutions was monitored during each test with portable conductivity and pH meters (WTW 314i), while samples of each solution were taken by a 5 mL syringe directly from the tank.

Table 2
Properties of cation (CEM) and anion (AEM) exchange membranes used in this work [42].

Membrane	Identification	Wet membrane thickness [μm]	Areal resistance[a] [Ω cm^2]	Permselectivity [%]	IEC[b] [meq g^{-1}]	Burst strenght [psi]
CEM	CR61N	300	3.6	95	2.20	95
AEM	AR103N	300	2.8	92	2.37	95
AEM-treated	AR103N-tr.	n.a.	n.a.	n.a.	n.a.	n.a.

n.a. not available.
[a] Measured in 0.1 mol L^{-1} NaCl solution.
[b] IEC refers to meq dry^{-1} g of resin.

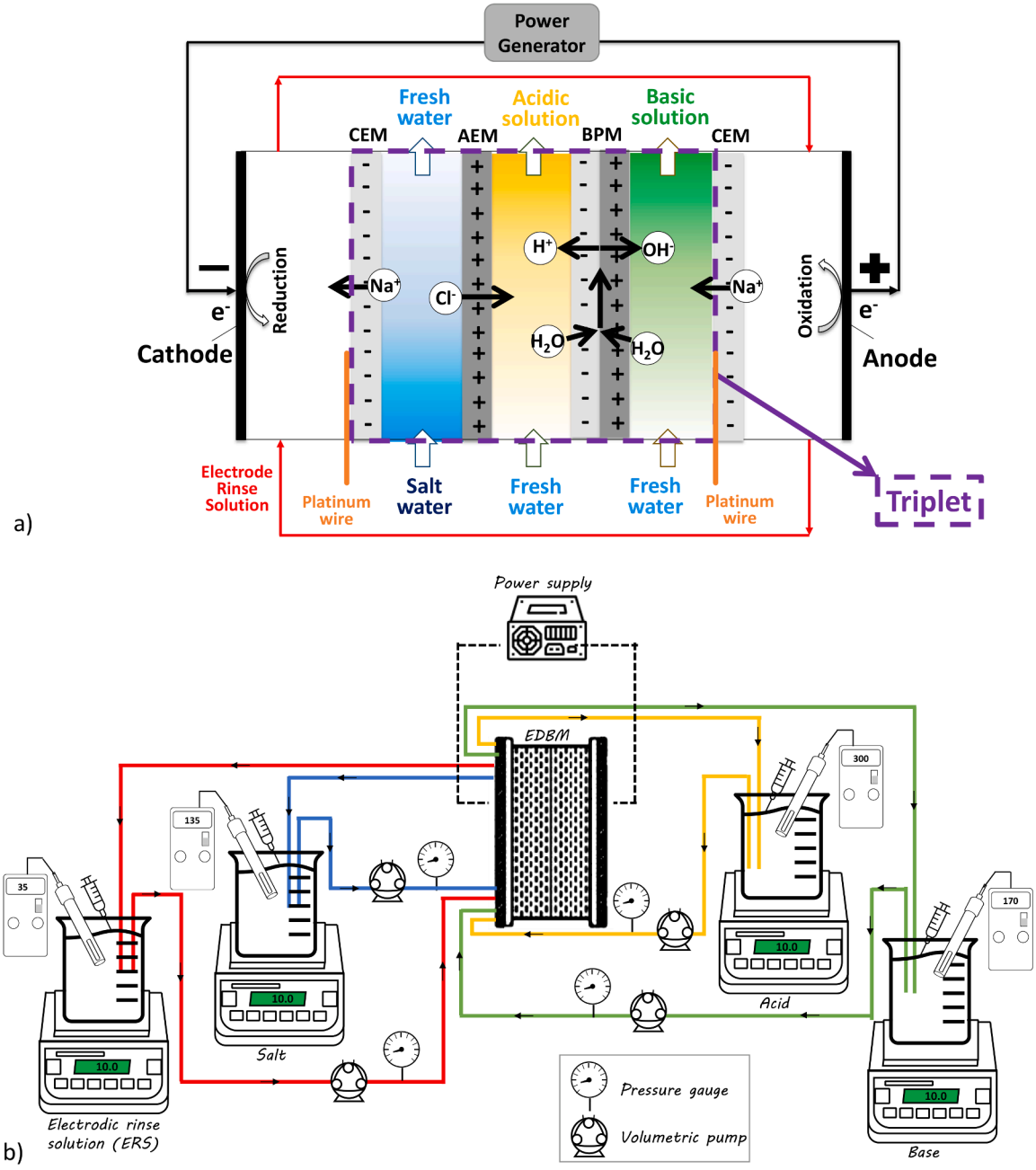

Fig. 1. Schematic representation of a) EDBM stack, including platinum wires (adapted from [43]), and b) laboratory EDBM setup and auxiliaries.

2.2. Experimental procedure and analytical techniques

After each stack assembly, external and internal leakage tests were conducted for at least one hour in closed-loop configuration with demineralized water into all compartments (1 L) to ensure a negligible leakage percentage (less than 5 % of the relative mass variation in one hour). Furthermore, the leakage test was repeated after each experiment to monitor any mass variation in time. When high leakage values (i.e.

Table 3
Brine composition for the salt compartment considering the 4 cases: i) Reference NaCl, ii) Case A concentrated brine, iii) Case B, diluted brine, iv) Case C, diluted alkaline brine.

	Reference NaCl only	Case A Concentrated brine	Case B Diluted brine	Case C Diluted alkaline brine
Na^+	2.0 mol L^{-1}	3.88 mol L^{-1}	1.13 mol L^{-1}	1.23 mol L^{-1}
Cl^-	2.0 mol L^{-1}	2.70 mol L^{-1}	0.91 mol L^{-1}	0.91 mol L^{-1}
SO_4^{2-}	–	0.74 mol L^{-1}	0.14 mol L^{-1}	0.14 mol L^{-1}
K^+	–	0.37 mol L^{-1}	0.06 mol L^{-1}	0.05 mol L^{-1}
OH^-	–	–	–	0.10 mol L^{-1}

greater than 5 % of the relative mass variation in one hour) were obtained, the stack was disassembled and re-assembled by replacing IEMs and/or spacers to fix the problem.

Experiments were carried out in closed-loop (i.e. batch) configuration with an initial volume of 1 L for both the alkaline and acidic solutions, 1.5 L for the brine and 2 L for the ERS, respectively. At the beginning of each test, the solutions were fed into the empty EDBM stack, and the Open Circuit Voltage (OCV) was measured. Subsequently, a fixed current density of 300 A m^{-2} was applied in all the tests for ~ 90 min to ensure reaching at least the target of 1 mol L^{-1} OH^- in the alkaline compartment for all the tested conditions. Longer test duration would bring to only slight increase in the outlet concentration, while significantly affecting the energetic performance of the stack, thus they are not of practical interest and have not been explored. The mass, conductivity, temperature, pH and voltage time-variation was recorded and analysed. Approximately six samples were taken per compartment (24 in total) using syringes. A sampling volume of 5 mL was chosen as a good compromise in order to i) not influence the mass variation during the test and ii) collect enough volume to perform a complete analysis by titration and ion chromatography. In particular, titrations were performed manually with standard solutions of 0.1 mol L^{-1} HCl, 0.05 mol L^{-1} Na_2CO_3, and 10 % w/w Methyl Orange solution (ACS dye content 85 % w/w, SIGMA-ALDRICH) as the visual pH indicator. Ion Chromatograph (Metrohm 882 compact IC plus) with anion (Metrosep A Supp 5 – 250/4.0) and cation (Metrosep C 4 – 250/4.0) columns was used to measure the concentration of anions and cations in the samples. The mobile phase of the cation and anion columns of the chromatograph were 5.5 mmol L^{-1} H_3PO_4 and a mixture of 3.2 mmol L^{-1} Na_2CO_3 and 1.0 mmol L^{-1} $NaHCO_3$, respectively.

2.3. Experimental plan

The experimental plan focused on the study of the stack performance and membrane properties, such as apparent transport number and ions selectivities, as a function of the synthetic brine composition (containing

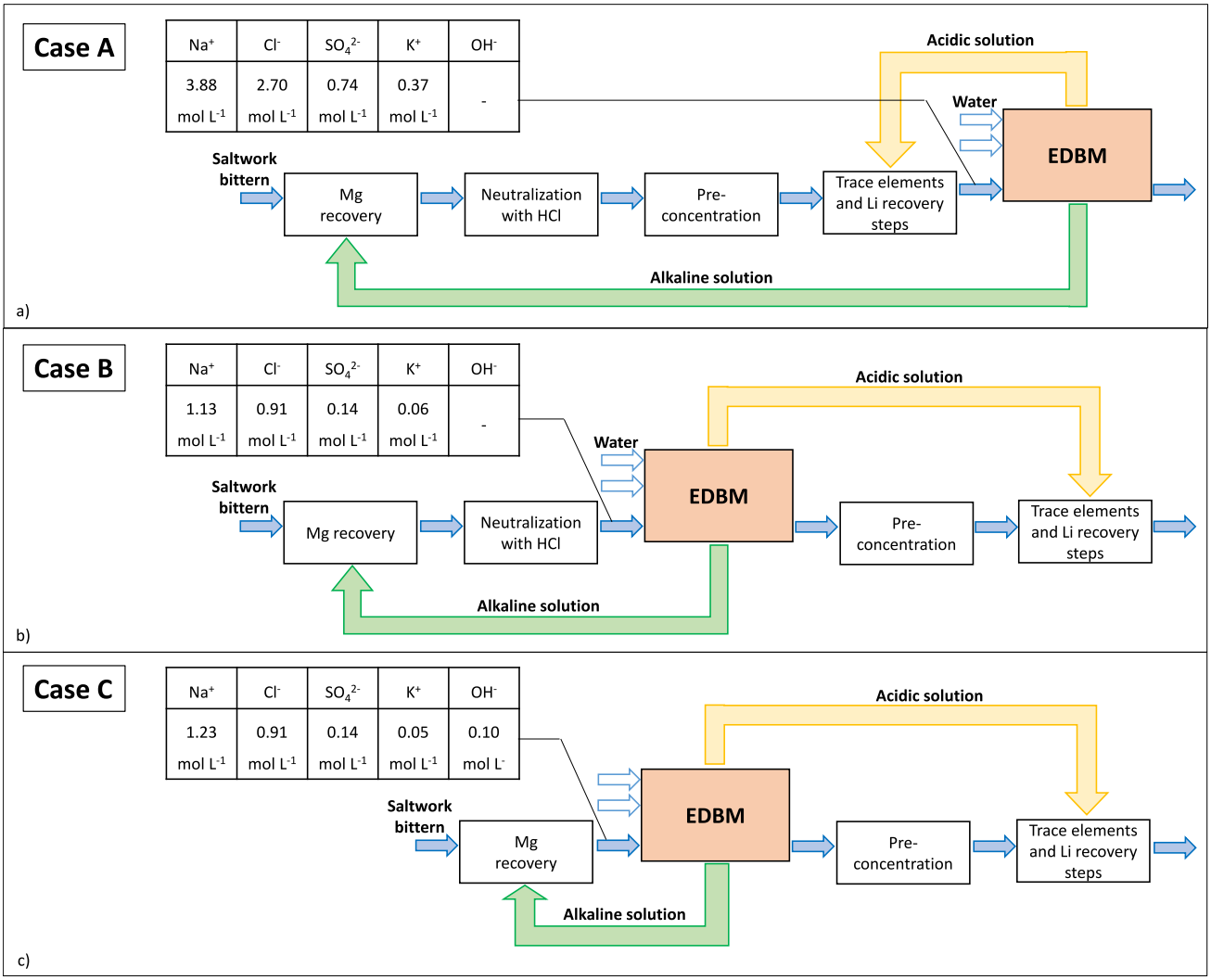

Fig. 2. Simplified schematic representation of the SEArcularMINE European project [24] treatment chain across different case studies corresponding to different positions of the EDBM unit.

a mixture of cations and anions: Na^+, K^+, Cl^-, SO_4^{2-}, OH^-) fed into the salt compartment of the EDBM unit. Table 3 reports the four different brine compositions, hereafter regarded as cases A, B and C, representing the different positions the EDBM unit can occupy in the saltwork bitterns valorisation treatment chain of the EU project SEArcularMINE [24]. Particularly as shown in Fig. 2, these are associated with the position after the Ca and Mg removal step (Case C in Fig. 2c), or the point after the post-neutralization step after Ca and Mg removal (Case B in Fig. 2b) and the position after the pre-concentration step of the Mg and Ca free bittern (Case A in Fig. 2a) of the SEArcularMINE saltwork bitterns valorisation treatment chain [24]. These cases represent a wide range of brine compositions from very concentrated brine (i.e., Case A) to more diluted brine (i.e., Case B). Specifically, the Case C brine differs from the Case B due to the addition of 0.1 mol L^{-1} NaOH; in fact, in the SEArcularMINE framework, the saltwork brine can contain OH^- ions due to the magnesium recovery step, which is performed by mixing brine and NaOH solutions. This third operating condition of Case C has a double purpose: i) exploring the possibility of neutralising the brine by exploiting the undesirable diffusion of H^+ ions from the acidic to the salt compartment, and ii) investigating whether a background concentration of OH^- in the brine, albeit moderate, can alter the stack performance. Tests with ionic mixtures were compared to a reference case with NaCl as single electrolyte.

Solutions were fed at a mean channel flow velocity of 7 cm s^{-1}, as suggested by the manufacturer, which corresponded to a volume flow rate of 890 mL min^{-1} for the acidic, alkaline and salt solutions and of 704 mL min^{-1} for the ERS. Tests were conducted at an initial concentration of 0.05 mol L^{-1} of HCl and NaOH for the acidic and alkaline solutions, respectively, to reduce the solutions' electrical resistance in the first part of the test.

During the experimental campaign, several tests were repeated to verify the experimental reproducibility of tests. The average standard deviations are shown in the graphs as error bars. In addition, with regard to ion analysis, the charge balance in each sample was verified to be within a relative error of less than 5%. The mass balances on each ion at varying times during the test were checked by taking into account the potential transport of the ions between the various compartments and their removal from the system with sampling volume.

2.4. Data analysis

This section focuses on data analysis and the assumptions made when treating the results. The first section (2.4.1) discusses ion transport across membranes in the presence of multi-ionic solutions. The second section (2.4.2) defines some performance parameters that will be used to compare results obtained with different feed solutions.

2.4.1. Ion transport across membranes in multi-ionic systems

The presence of several ionic species in the salt compartment causes different EDBM behaviour compared to the scenario with only NaCl solutions. From the EDBM experiments, the mass of ions transported from/in each specific tank (acid, alkaline, salt) were calculated, and, consequently, the relevant flux across the membranes.

Fig. 3 reports a simplified scheme, including the main ion fluxes across IEMs. Particularly, the fluxes of ions different than protons and hydroxide, can be attributed to their transport across either the monopolar CEM or AEM (from salt compartment to base/acid compartment), while it is considered negligible across the BPM layers. Indeed, it was assumed that the predominant fluxes across the BPM layers are related to the water dissociation reaction, which leads to protons and hydroxide ions passage. This assumption, although simplistic, is reasonable since the limiting current associated with the transport of the other ions from the interlayer of the BPM towards the adjacent acid and alkaline channels is considered small enough to be negligible [44].

Based on this assumption, the ion fluxes $J_{i,\tau}^{AEM}$ and $J_{i,\tau}^{CEM}$ (in mol m^{-2} s^{-1}) across the monopolar membranes (i.e., AEM and CEM) were calculated at a generic time τ, as described by Eqs. (1), (2):

$$J_{i,\tau}^{AEM} = \frac{\left(V_{acid,\tau} \bullet C_{i,acid,\tau} - V_{acid,\tau=0} \bullet C_{i,\ \mathrm{acid},\tau=0}\right)}{NS\tau} \quad (1)$$

$$J_{i,\tau}^{CEM} = \frac{\left(V_{base,\tau} \bullet C_{i,base,\tau} - V_{base,\tau=0} \bullet C_{i,\ \mathrm{base},\tau=0}\right)}{NS\tau} \quad (2)$$

where τ (s) is the generic time, C (mol L^{-1}) and V (L) are the concentration of ion i and the volume of the generic compartment (acid or base), N is the number of triplets and S (m^2) is the active membrane area. Specifically, except for protons and hydroxide ions, fluxes across AEM or

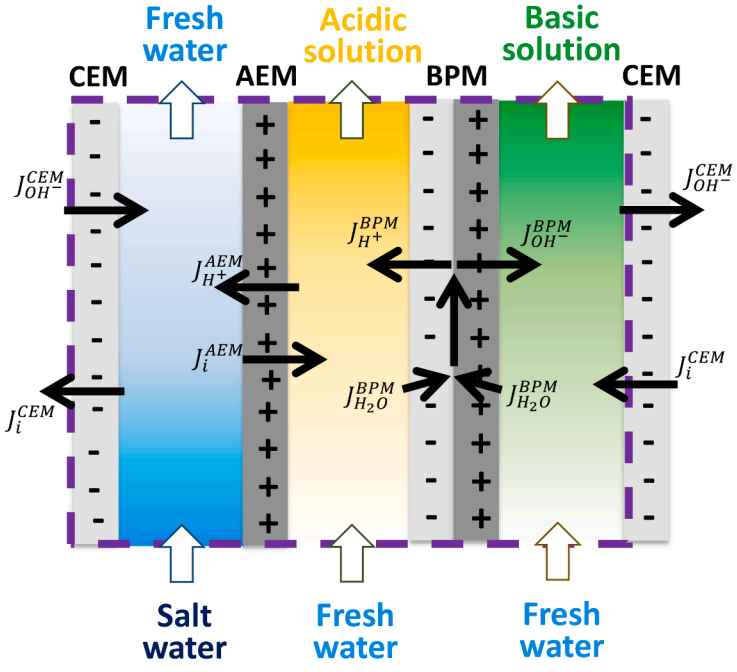

Fig. 3. Simplified representation of the EDBM triplet including the main ion fluxes and the expected directions (adapted from [16]).

CEM were estimated using the concentration values of each ion and the solution volumes for each compartment. These fluxes calculations should be regarded as representing apparent net fluxes, including conduction and diffusion transport mechanisms.

Due to undesirable phenomena, such as H^+ and OH^- ion back-diffusion and non-ideal perm-selectivity of IEMs, part of the H^+ and OH^- generated at the bipolar membrane interlayer were transported across AEM and CEM, respectively, thus leading to neutralisation and pH variation of the salt compartment. The fluxes of H^+ and OH^- towards AEM and CEM, $J^{AEM}_{H^+,\tau}$ and $J^{CEM}_{OH^-,\tau}$ respectively, were thus defined as the difference between proton and hydroxide ions generation at the bipolar, $J^{BPM}_{H^+,\tau}$ and $J^{BPM}_{OH^-,\tau}$, and the fluxes estimated from the experimental concentrations. In formula $J^{AEM}_{H^+,\tau}$ and $J^{CEM}_{OH^-,\tau}$ were calculated as described by Eq. (3)–(4):

$$J^{AEM}_{H^+,\tau} = J^{BPM}_{H^+,\tau} - \frac{\left(V_{acid,\tau} \bullet C_{H^+,acid,\tau} - V_{acid,\tau=0} \bullet C_{H^+,\ acid,\tau=0}\right)}{NS\tau} \quad (3)$$

$$J^{CEM}_{OH^-,\tau} = J^{BPM}_{OH^-,\tau} - \frac{\left(V_{base,\tau} \bullet C_{OH^-,base,\tau} - V_{base,\tau=0} \bullet C_{OH^-,\ base,\tau=0}\right)}{NS\tau} \quad (4)$$

The flux of H^+ and OH^- across the BPM (i.e., unitary transport numbers), $J^{BPM}_{H^+,\tau}$ and $J^{BPM}_{OH^-,\tau}$ (mol m^{-2} s^{-1}), can be estimated by Eq. (5):

$$J^{BPM}_{H^+,\tau} = J^{BPM}_{OH^-,\tau} = \frac{I/S}{F} \quad (5)$$

where I (A) is the applied current and F (96,485C mol^{-1}) is the Faraday Constant. Since the tests were conducted at constant current, these fluxes were also constant throughout the duration of the test. This assumption, although simplistic, can be reasonable since the parasitic currents via manifolds, that usually reduces the process current efficiency, are negligible at low number of triplets (i.e., 5 in this study), and the transport of the other ions towards the bipolar membrane can be considered negligible at this high current density [44].

Under these assumptions, the total ion flux across AEM and CEM, $J^{AEM}_{tot,\tau}$ and $J^{CEM}_{tot,\tau}$ (in mol m^{-2} s^{-1}) at a generic time τ are given by Eq. (6)–(7):

$$J^{AEM}_{tot,\tau} = \sum_i J^{AEM}_{i,\tau} + J^{AEM}_{H^+,\tau} \quad (6)$$

$$J^{CEM}_{tot,\tau} = \sum_i J^{CEM}_{i,\tau} + J^{CEM}_{OH^-,\tau} \quad (7)$$

where the subscript i refers to the different ions used in the multi-ionic salt solution (K^+, Na^+, Cl^- and SO_4^{2-}).

For the sake of brevity, osmotic and electro-osmotic fluxes were described in the Supplementary Information section.

For the first time for EDBM, an effective methodology is proposed utilizing solution compositions and ion fluxes across IEMs to calculate apparent transport numbers and selectivities. This approach provides valuable and comprehensive insights into ion transport across IEMs through relatively simple, whole-stack experiments.The apparent transport number of a generic ion i across a monopolar membrane at a generic time τ, $t_{i,IEM,\tau}$, was defined as the ratio between the ion flux and the total ion flux across the generic IEM, as described by Eq. (8):

$$t_{i,IEM,\tau} = \frac{J^{IEM}_{i,\tau}}{J^{IEM}_{tot,\tau}} \quad (8)$$

where $J^{IEM}_{i,\tau}$ and $J^{IEM}_{tot,\tau}$ (in mol m^{-2} s^{-1}) are the ion flux and the total flux across the generic monopolar membrane.

The ion selectivity for a specific IEM to a generic ion, i, with respect to a reference ion at a generic time τ was defined as the ratio between the fluxes of the ion, i, and a reference ion, *ref*, normalized for the ratio between the concentrations of the same ions present in the salt channel. In formula, $Sel_{\frac{i}{ref},IEM,\tau}$ was calculated as by Eq. (9):

$$Sel_{\frac{i}{ref},IEM,\tau} = \frac{J_{i,IEM,\tau}/J_{ref,IEM,\tau}}{C_{i,salt,ave}/C_{ref,salt,ave}} \quad (9)$$

where $C_{i,salt,ave}$ (mol L^{-1}) and $C_{ref,salt,ave}$ (mol L^{-1}) are the average concentrations over the test duration for the generic ion, i, and the reference ion in the salt compartment.

2.4.2. Performance parameters of the EDBM unit

All performance parameters in this study were referred to "produced NaOH", which represents the process's highest added-value product. In order to compare various multi-ionic solutions, performance parameters were normalized to the equivalent amount of NaOH, assuming that all OH^- ions were associated with Na^+ ions. This normalization was applied consistently, even when the resulting alkaline solution contained a combination of NaOH and KOH. This assumption is reasonable given the low concentration of K^+ compared to Na^+ in all salt solutions used (see Table 3).

Specific Energy Consumption, *SEC* (kWh kg^{-1}_{NaOH}), represents the energy required to produce 1 kg of NaOH. It is defined by Eq. (10):

$$SEC = \frac{I \cdot \int_{\tau=0}^{\tau} U_{Pt} \cdot d\tau}{3600 \bullet \left(C_{OH^-,\tau} \bullet V_{base,\tau} - C_{OH^-,\tau=0} \bullet V_{base,\tau=0}\right) M_{NaOH}} \quad (10)$$

where I (A) and U_{Pt} (V) are the applied current and the corresponding Platinum wires voltage, respectively, τ (s) is the process time, C_{OH^-} (mol L^{-1}) and V_{base} (L) are the OH^- concentration and the alkaline volume, respectively; M_{NaOH} (g mol^{-1}) is the NaOH molecular weight, and the subscript τ refers to a generic time. Solutions volumes variation along the test was estimated from the experimental measurement of mass, using mass densities, calculated using PhreeQC software (PhreeQC Interactive 3.7.0–15749) [45] with the Pitzer database. A relative error less than 4% was obtained when comparing model vs experimental values evaluated at the beginning and at the end of the test.

It is worth noting that the *SEC* values reported in this work refer to the voltage measured at the platinum wires, excluding the voltage drop at the electrodes. Indeed, the former is a more reliable estimate with reference to possible scale-up analysis to pilot or industrial scale units, in which the voltage drop across the electrode compartments would be negligible. More information on the difference between the electric potential at the overall stack and platinum wires can be found in the Supplementary Information section.

Current efficiency, *CE* (%), represents the fraction of the total electric current effectively converted in OH^- in the alkaline compartment. It is defined by Eq. (11):

$$CE = \frac{\left(C_{OH^-,\tau} \bullet V_{base,\tau} - C_{OH^-,\tau=0} \bullet V_{base,\tau=0}\right) \cdot z\, F}{I \cdot N \cdot \tau} 100 \quad (11)$$

where z is the ion valence.

Specific Productivity, SP (kg_{NaOH} m^{-2} y^{-1}), represents the amount of NaOH produced by the unit of membrane area in one working year (assumed equal to 8,000 h in this work). In formula, SP was calculated by Eq. (12):

$$SP = \frac{M_{NaOH} \cdot \left(C_{OH^-,\tau} \cdot V_{base,\tau} - C_{OH^-,\tau=0} \cdot V_{base,\tau=0}\right) \cdot 8,000}{1,000 \cdot N \cdot 3 \cdot S \cdot \frac{\tau}{3600}} \quad (12)$$

where S (m^2) is the active membrane area and 3 the number of membranes per triplet, while τ (s) is the generic time of the experiment.

3. Results and discussion

Results are here presented according to three sub-sections. The first one (3.1) focuses on the comparison of the production capacity of acidic and basic solutions for several feeds (either NaCl only or multi-ionic mixtures). Then, the analysis of membrane properties, as well as

apparent transport numbers and selectivities, is discussed, focusing on the use of multi-ionic solutions (Section 3.2). Finally, performance parameters in terms of both energy consumption and productivity is presented (Section 3.3).

All analyses were performed with four types of brine compositions (i.e., Case A, Case B, Case C and Reference), although some of the results are reported in the Supplementary Information file for the sake of brevity.

3.1. Production of OH^- and H^+ using multi-component solutions

The first results section focuses on comparing the production capacity of acidic and basic solutions for several feeds (NaCl only or multi-ionic mixtures).

Fig. 4 shows the results obtained at 300 A·m^{-2} with the four different salt solutions tested in terms of OH^- concentration profile versus time. Similarly, H^+ concentration profiles were obtained, but they are reported in Supplementary Data (Fig. S1a).

Theoretically, assuming that all the electric current is being used to generate acid and base and that no volume variation occurs in the tanks ("ideal case"), the concentration of OH^- should increase linearly along the test (dashed lines in Fig. 4a). However, it can be observed that only during the first 10–15 min the concentrations of OH^- with the four solutions followed the ideal behaviour. Then, the rate of OH^- concentration increase diminished over time, especially towards the end of the experiment, thus indicating a reduction of ~ 50–70 % in the current efficiency (see Fig. 4a), likely due to the presence of non-ideal phenomena such as counter-diffusion of ions and water transport (osmosis and electro-osmosis) that become significant, especially at high concentrations. Since the unit contains a low number of triplets (i.e., 5 in this study), the parasitic currents via manifolds are negligible. Interestingly, synthetic multi-ionic solutions showed similar or better performance in terms of final concentration compared to the reference case. The final concentrations achieved slightly higher values ranging from 1.15 ± 0.02 mol L^{-1} to 1.44 ± 0.01 mol L^{-1} OH^-. In addition, when comparing the trends of H^+ and OH^-, it can be observed that the concentrations of H^+ (see Figure S1) tended to be lower than the ones of OH^-, which can be related to the transport of H^+ from the acid to the salt compartment due to its lower size and higher mobility (0.282 nm and 9.31·10^{-9} m^2 s^{-1}) than the ones for OH^- (0.300 nm and 5.27·10^{-9} cm^2 s^{-1}) [46]. With regard to Case C, it was possible to exploit the undesired passage of H^+ to neutralize the initially alkaline salt solution (0.1 mol L^{-1} OH^-) to a pH of ~ 1 at the target of 1 mol L^{-1} OH^-.

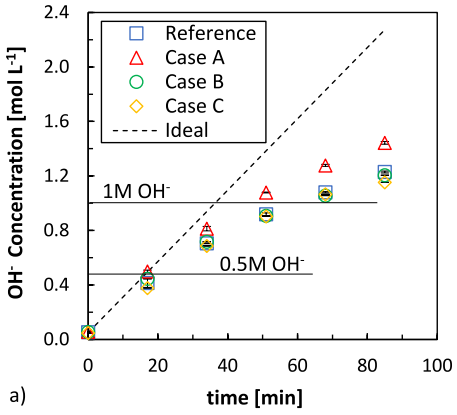

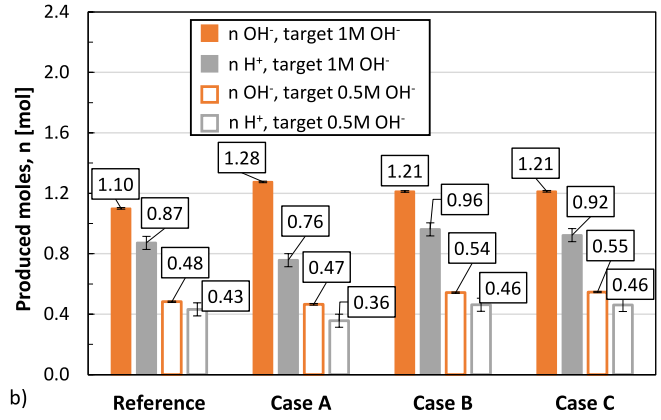

Fig. 4. A) concentrations of OH^- achieved as a function of time and b) moles produced of OH^- and H^+ at the targets of 1 and 0.5 mol L^{-1}. Tests were performed at 300 A·m^{-2}. The dashed line indicates the ideal concentration profile.

Similarly, Fig. 4b shows that slightly different number of produced moles arose when comparing the different case studies at the two targets 0.5 and 1 mol L^{-1} OH^-, mostly related to different water transport ratios. In fact, in all tests a higher final volume of alkaline solution was recorded (due to a preferential transport of water from the salt towards the base compartment by osmosis and electro-osmosis), thus producing more than 1 mol of OH^- at the target 1 mol L^{-1} OH^-. The two contributions to the total water fluxes are reported in the Supplementary Information (see Figures S2-S4) for Case C tests, showing the contribution of electro-osmosis flux (from the salt to the acid and base compartments) constituted more than 80% of total water flux. Overall, the produced moles of OH^- ranged from 1.10 (Reference case) to 1.28 (Case A) and from 0.47 (Case A) to 0.55 (Reference case) at the targets of 1.0 and 0.5 mol L^{-1}, respectively. In addition, a lower net production of H^+ was observed respect to OH^- due its transport towards the salt compartment.

3.2. Multi-ionic transport during EDBM operation

In this section, the properties of the membranes, including transport numbers and selectivity, are firstly examined by analysing the behaviour of the EDBM unit over time under Case A conditions. Supplementary Data Section includes additional data on Cases B and C (Fig. S4–S7). Then, all case studies are compared at the same target concentration of 1 mol L^{-1} OH^-.

In Case A, all non-ideal phenomena are exacerbated by the high ion concentration in the solution. Fig. 5 shows the ion concentration profiles over time for the acid, alkaline and salt channels in Case A.

The ion concentrations in both the acid and alkaline compartments increased over time, whereas in the salt channel, the ion concentrations decreased. For all ions, a net positive flux (and, thus, inflow, according to the adopted sign convention) was observed in the acid and base channels, resulting from both migrative and diffusive fluxes. Fig. 5 shows that the concentration gradient (i.e., $C_{i,salt} - C_{i,acid}$ or $C_{i,salt} - C_{i,base}$) was always positive, indicating a diffusive flux from the salt channel into the acid and alkaline channels. Furthermore, the concentration gradient decreased over time, reducing the diffusive transport contribution.

Fig. 5 shows a greater increase in the concentration of Cl^- compared to SO_4^{2-} in the acid compartment. In the alkaline channel, Na^+ exhibited a higher increase compared to the other ions present. Additional transport aspects can be considered by calculating the apparent ion transport numbers using Eq. (8), which accounts for both conduction and diffusion transport mechanisms. The profiles over time for the ion transport numbers for the AEM and CEM are depicted in Fig. 6a and b, respectively.

The results in Fig. 6a demonstrate that the primary ion transported through the AEM was chloride, with an ion-transport number range of 42–63 %, followed by protons with a range of 24–45 %. Over time, the proton transport number increased across the AEM, indicating that higher acid concentrations reduced the proton-blocking capacity of the membranes. As acid concentration increased, the proton transport number increased until it reached the same value as the chloride transport number. The increasing trend of the proton transport number

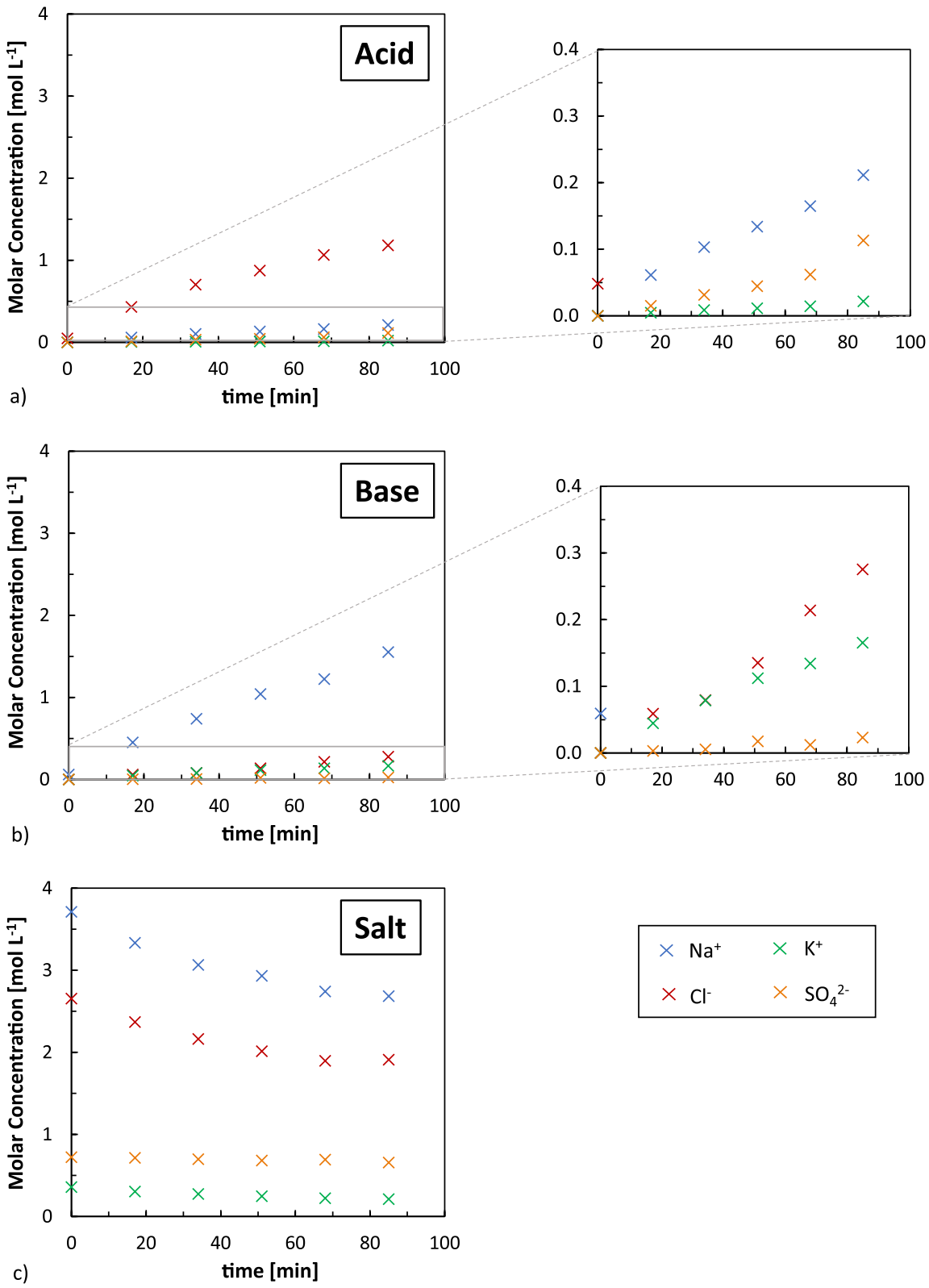

Fig. 5. Concentration of single ions (Na^+, Cl^-, K^+, SO_4^{2-}) as function of time in the a) acid, b) base, and c) salt compartments. Case study A. Current density: 300 A·m^{-2}.

profile over time was likely due to the increased diffusion of acid towards the salt channel. Indeed, the proton concentration, along with its concentration gradient across the AEM, reached a plateau towards the conclusion of the experiment (refer to Figure S1).

Furthermore, there was a slightly decreasing trend in the sodium transport number through the AEM, with average values of 9 %.

Surprisingly, despite the double negative valence of the SO_4^{2-} ion, it showed low passage through the AEM (only 2–4 %). This phenomenon

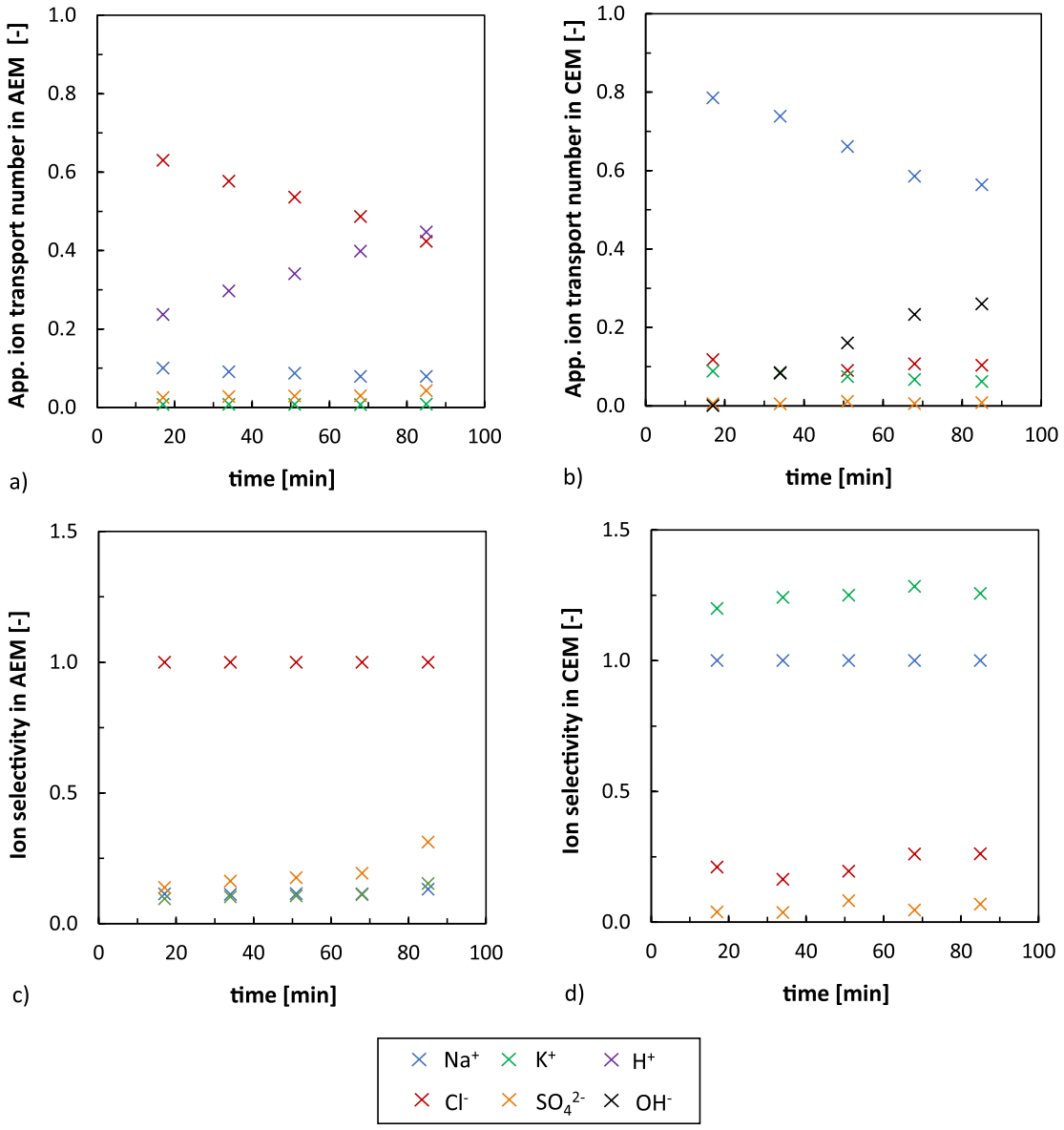

Fig. 6. Apparent ion transport numbers for a) AEM and b) CEM and ion selectivity profiles for c) AEM and d) CEM as function of time. Case study A. Current density: 300 A·m^{-2}.

may be attributed to the low ionic mobility of SO_4^{2-}, which may outweigh the effect of its double valence. Potassium transport was negligible (less than 0.8 % at a target concentration of 1 mol L^{-1} OH^-), likely due to the low concentration in the salt feed compartment. Overall, there was an approximately constant transport number for SO_4^{2-}, Na^+, and K^+ and a higher variation over time for chloride and proton ions.

Similar to the AEM, the CEM could not completely block hydroxide ions, which were partially transported and neutralized in the salt compartment. The OH^- and Na^+ had opposite transport trends. As the hydroxide ion (OH^-) concentration increased, a higher relative transport of OH^- through the CEM was observed, accompanied by a decrease in the Na^+ transport number. The transport numbers for SO_4^{2-}, K^+, and Cl^- remained relatively constant over time. The most excluded ion through the CEM was SO_4^{2-} (transport number less than 1 %). Indeed, SO_4^{2-} is a co-ion for the CEM and has a double electric charge, making their passage through a CEM unfavourable. Furthermore, the salt compartment exhibited a higher concentration of chloride ions compared to sulfate ions, with the latter demonstrating a relatively low transport number (below 15 %). Although potassium was a counter-ion and chloride a co-ion for the CEM, they showed similar transport numbers, which may be due to the large concentration difference between the two ions in the salt feed stream.

It is important to note that ion transport numbers provide limited information, as they depend heavily on ion concentrations in solutions. High concentrations of an ion in solution are associated with high transport numbers. Therefore, selectivities of ionic species in relation to a reference ion (Eq. (9)) were calculated, specifically, for the AEM in relation to chlorides (Fig. 6c) and for the CEM in relation to sodium (Fig. 6d) to provide a comprehensive overview. Selectivities for reference values were equal to 1. The AEM showed almost constant sulphate selectivity over time, equal to ~ 0.20. The relatively low sulphate selectivity value may be due to the low mobility of SO_4^{2-} compared to Cl^-. As a result, the AEM provided up to seven times higher selectivity of chlorides than sulphates. Additionally, the AEM selectivities for both sodium and potassium ions remained relatively constant and essentially overlapped, indicating that both cations permeated through the membrane with similar efficiency. Although sodium exhibited a higher transport number through the AEM (refer to Fig. 6a), its selectivity was

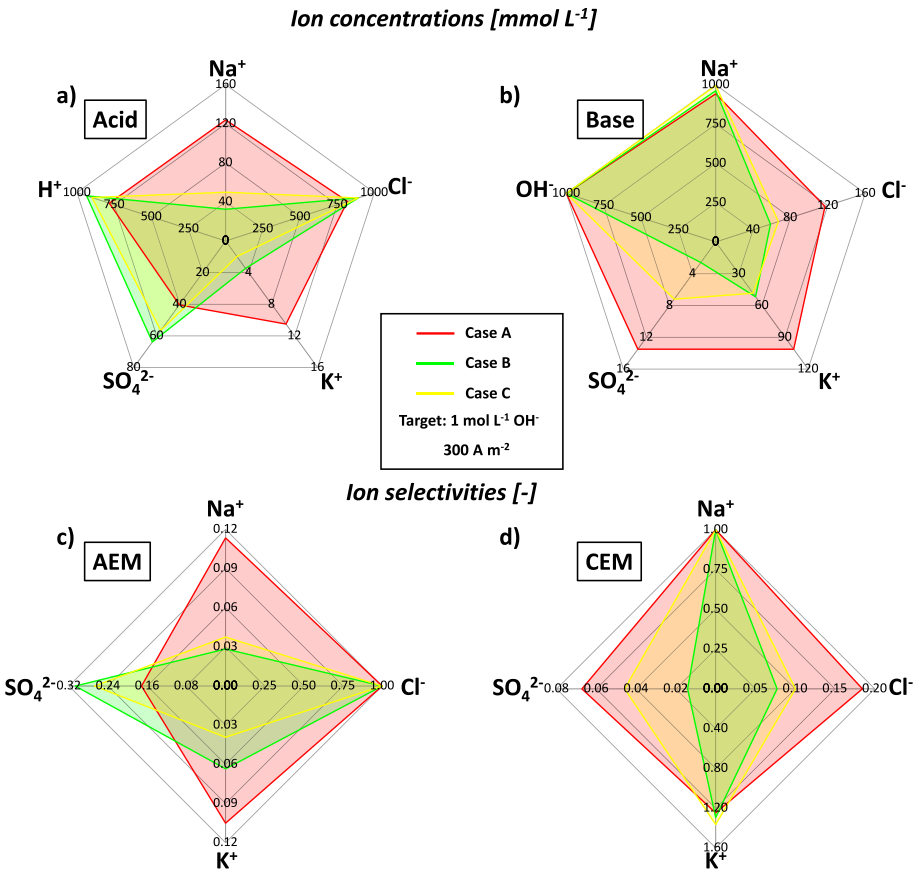

Fig. 7. Ion concentration for a) acid and b) base compartments and ion selectivity for c) AEM and d) CEM at 1 mol L^{-1} OH^- target, for Cases A, B and C. Current density: 300 $A{\cdot}m^{-2}$.

still lower than that of sulfate, consistent with the expectations based on Donnan exclusion. Specifically, the selectivity of SO_4^{2-} was approximately twice that of Na^+.

In the case of the AEM, the reference counter-ion, chloride (Cl^-), demonstrated the highest selectivity. This can be attributed to the enhanced facility of chloride ions traversing the membrane compared to sulfate ions. Conversely, for the CEM, potassium demonstrated the highest selectivity, with an average value approximately 20 % greater than that of sodium, despite its lower concentration in the saline feed. This enhanced selectivity of the CEM for potassium can be ascribed to the ion's higher mobility relative to sodium, stemming from its larger ionic radius and smaller hydration shell [47], which decreased the friction experienced while moving through the aqueous solution. The CEM exhibited a selectivity for Cl^- that was roughly four times greater than that of SO_4^{2-}, a behavior attributed to the double valence of SO_4^{2-} compared to Cl^- and its increased steric hindrance.

In summary, the ion selectivities in both AEM and CEM remained largely constant during the experimental tests, suggesting that the membranes had stable performance over time once the tests commenced.

A performance analysis was conducted at the target 1 mol L^{-1} OH^- concentration under the different scenarios evaluated, namely Case A, B and C (see Fig. 7).

Fig. 7a and b depict the ion concentrations in the acidic and alkaline channels, respectively. When the target concentration of 1 mol L^{-1} OH^- was attained, Case A exhibited the minimum proton concentration in the acid compartment, whereas Case B showed the maximum value. Indeed, the higher initial salt concentrations in the feed of Case A may have intensified the diffusive flux of protons from the acid to the salt channel. In the alkaline compartment, sodium was the predominant ion transported from the salt to the alkaline channel across the CEM, while the selectivity of K^+ was higher than that of Na^+ for all case studies (refer to Fig. 7d).

Conversely, with regard to the AEM, Case B showed almost twice the selectivity for SO_4^{2-} (i.e., 0.31) compared to Case A (i.e., 0.16), as the lower chloride concentration in the feed led to its faster depletion and the subsequent predominance of sulphates transport into the acid channel (see Fig. 7c). In general, the elevated ionic strength of the saline solution in Case A resulted in a substantial increase in the co-ion selectivities for both IEMs. This implied that more concentrated solutions may contribute to a decline in product purity, as the produced acidic or alkaline solutions will have higher contamination from potentially undesired ions. The increased co-ion selectivity primarily stemmed from the enhanced concentration gradient of the ionic species across the membranes, which subsequently led to a higher diffusive flux from the saline to the acid/alkaline compartment. Consequently, the impurities (i.e., the co-ions mass fraction) of the acidic and alkaline solutions in Case A was increased by an average of 42 % and 28 % in comparison to cases B and C, respectively. Specifically, for Case A, the acid compartment contained impurities of Na^+ and K^+ with mass fractions of 7.6 % and 1.0 %, respectively, while SO_4^{2-} constituted 10.2 %. When the feed salinity was reduced (Cases B and C), the impurities of Na^+ and K^+ decreased to 2.7 % and 0.35 %, respectively, whereas the mass fraction of SO_4^{2-} remained at 10.7 % for the acid. Similarly, in the alkaline solution, the highest impurities were observed in Case A (8.9 % Cl^-, 1.3 % SO_4^{2-}, and 8.4 % K^+), whereas they reduced by approximately half for Cases B and C (5.9 % Cl^-, 1.0 % SO_4^{2-}, and 4.9 % K^+). These findings are consistent with the impurity levels reported in the literature for similar feed salinities (refer to Table 1).

This analysis suggests that the EDBM offers the ability to produce both acidic and alkaline solutions, as well as concentrate or dilute specific ionic species relative to the others. For example, using a diluted

brine solution (e.g., Case B or C) significantly decreased chloride concentration (from 1 mol L^{-1} to 0.25 mol L^{-1}) over time, while the sulphate concentration remained relatively stable at around 0.12 mol L^{-1}.

3.3. Performance parameters of the EDBM unit

Fig. 8 reports OH^- *CE* (graph a), platinum wires voltage (graph b) and SEC for the alkaline compartment (graph c) as function of time. For all case studies, *CE* (Fig. 8a) reached considerably high values in the first part of the test (up to 95–99 %). As time progressed, the *CE* was reduced in all cases due to the effect of non-ideal phenomena such as ion diffusion, electro-osmosis and osmosis, enhanced by the higher acid and alkaline concentration. The reduction in *CE* can also be attributed to the non-ideal 100 % perm-selectivity of BPMs. In fact, the transport of Na^+ or Cl^- towards the BPM can substitute part of water transport and dissociation [44]. Both phenomena increased over time because of the concentration growth in the base and acid channels, resulting in a *CE* in all cases above 60 % at the end of the test. The use of a synthetic brine feed (i.e., a multi-ionic system) compared to the use of a NaCl solution did not lead to a significant impact on *CE*. Indeed, in comparison with the Reference case study (2 mol L^{-1} NaCl), when mixed-salt brine was used (i.e., Case A, B, and C), *CE* was comparable or even higher, as with Case A and Case C brines.

Fig. 8b shows the platinum wires applied voltage for all brine compositions studied. A reduction of the Pt wires voltage over time was observed in all conditions. The increase in acid and alkaline solutions concentration led to two different effects on voltage trend: i) the reduction of the ohmic resistance of two compartments per triplet (alkaline and acidic channels from 7.3 Ω cm^2 and 4.6 Ω cm^2 to 0.4 Ω cm^2 and 0.2 Ω cm^2) and ii) the increase in the Nernst potential. The former prevailed over the latter under the operating conditions tested, producing an overall reduction at the Pt wires voltage, observed in Fig. 8b. However, it may be noted that the most significant reduction occurred in the first part of the test (i.e., first 20 min), where the concentration of acid and base solutions increased from 0.05 mol L^{-1} to ~ 0.34–0.50 mol L^{-1}, thus significantly reducing the corresponding ohmic resistance. In contrast, the voltage decreased slowly in the second part of the test, showing that the Ohmic contribution was less significant and did not outweigh the Nernst contribution.

The use of a solution with a different concentration in the salt compartment had a negligible effect on the platinum voltage. This outcome was a result of the high concentration within the salt compartment, regardless of the feed composition, leading to a low electrical resistance. Upon analysing the electrical resistance, it was observed that at the beginning of the test for Case C brine (least concentrated), the salt compartment contributed to merely ~ 1 % of the triplet resistance (refer to Figure S6 in the Supplementary Section). The acid and base compartments were responsible for 7 % and 13 % of the triplet resistance, respectively, while the remaining part was related to the membrane resistances. Moreover, enhancing the ionic strength of the salt feed (i.e., transitioning from Case C to Case A) has a negligible impact on reducing the triplet resistance. Indeed, this resistance is not primarily attributed to the salt channel, which consistently exhibits high conductivity throughout the entire test. The high conductivity can be attributed to the high initial ions concentration, the larger initial salt volume (1.5 L for salt versus 1.0 L for acid and base), and the acidification of the salt compartment.

The SEC referred to the alkaline product trend (Fig. 8c) is proportional to the electric potential and inversely related to the *CE*, which both decreased over time. In the first part of the test, the SEC slightly

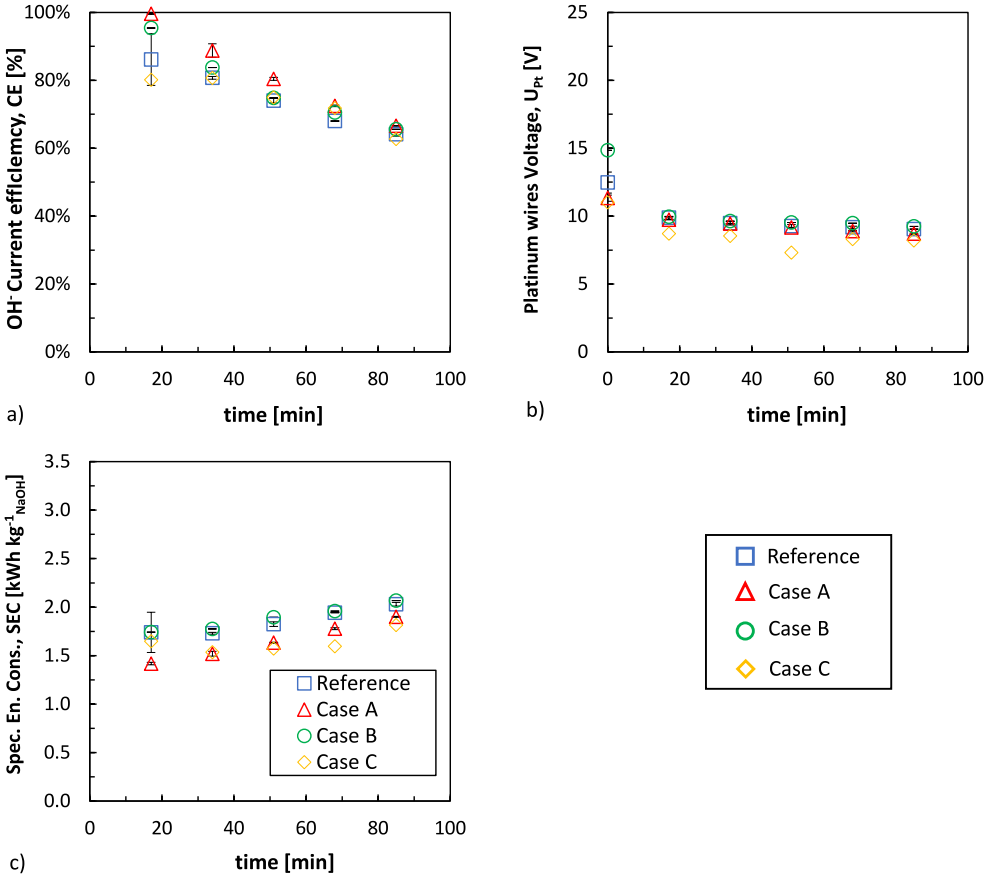

Fig. 8. A) current efficiency, b) platinum wires voltage, c) specific energy consumption as function of time. CE and SEC refer to the alkaline compartment. tests were performed with four different brine compositions (reference, Case a, Case b and Case c), at 300 A m^{-2}.

rose over time due to the reduction of the increasing rate in voltage, which partly counterbalanced the decrease in *CE*. Conversely, in the second part of the test, the faster SEC increase could be explained mainly by the faster decrease in *CE* and the lower voltage reduction rate. At the target of 0.5 mol L^{-1} OH^-, SEC values of ~ 1.42–1.75 kWh kg^{-1}_{NaOH} were achieved. Similarly, at the target of 1 mol L^{-1} OH^-, SEC values of ~ 1.60–1.94 kWh kg^{-1}_{NaOH} were obtained. The use of mixed-salt brines had no negative impact on energy consumption, as already observed for both *CE* and platinum voltage trends. Indeed, in most cases, the presence of a multi-ionic system slightly reduced SEC.

Fig. 9 reports the specific productivity, SP in kg_{NaOH} y^{-1} m^{-2}, as a function of the different investigated cases, for the two targets of 0.5 and 1 mol L^{-1} OH^-. Overall, SP ranged between 960 kg_{NaOH} y^{-1} m^{-2} (Reference) and 1,185 kg_{NaOH} y^{-1} m^{-2} (Case A), for 0.5 mol L^{-1} OH^- target, and between 850 kg_{NaOH} y^{-1} m^{-2} (Case B) and 990 kg_{NaOH} y^{-1} m^{-2} (Case A) for 1 mol L^{-1} OH^-.

These results are in line with the maximum and minimum current efficiencies achieved and confirmed that multi-ions solutions can increase EDBM performance.

Specifically, cases B, C, and the reference demonstrate similar *CE*, whereas Case A exhibited a higher value, which consequently resulted in a reduced SEC. The increased efficiency can be attributed to several factors, including the enhanced ionic strength of the solution, improved ion-exchange capacity of the membranes, and competitive ion migration effects. In multi-ion systems, the ion-exchange capacity of the membranes may be enhanced due to the cooperative interactions between various ions and the ion-exchange sites on the membrane surface. This can result in a more effective separation of ions in the EDBM process leading to an increase in *CE*. Finally, the presence of multiple ions can also lead to competitive ion migration effects, which can help in the selective separation of target ions. The competitive migration of ions can minimize the undesirable transport of co-ions, thereby improving the overall selectivity of the EDBM process.

In an ideal operating condition with no volume variation and a CE of 100 % (as reported in dashed lines in Fig. 2a and Fig. 3a), SP would be constant and only a function of the stack design (e.g. membrane area) and operating conditions (e.g., current density). For the present stack, the ideal *SP* was 1,194 kg_{NaOH} y^{-1} m^{-2} when operating at 300 A m^{-2} and independent of target concentration. Overall, when the target doubled, *SP* reduced by an average of 14 % and remained relatively high compared to the maximum value achievable under ideal conditions.

4. Conclusions

In this work, a novel approach for the experimental characterization of ion transport properties in IEMs in EDBM stacks for multi-ionic feed streams was presented. Four different multi-ionic brine compositions (containing Na^+, K^+, Cl^-, and SO_4^{2-} ions) were tested on SUEZ IEMs. The presence of multi-ionic solutions had a negligible effect on OH^- production compared to the case of a solution with NaCl only, with similar or slightly higher OH^- concentrations obtained in the former case. At a current density of 300 A m^{-2}, final OH^- concentrations of 1.15–1.44 mol L^{-1} were achieved. Electro-osmotic flux accounted for about 80 % of total flux in both channels, leading to volume variations in both acidic and alkaline compartments.

Regarding ions transport across IEMs, the diffusion of OH^- through the CEM occurred more slowly than that of H^+ through the AEM, so a net reduction in the pH of the salt solution was observed.

AEMs demonstrated SO_4^{2-} selectivity of ~ 0.15 at the target of 1 mol L^{-1} OH^-. This value was most likely due to the lower mobility of SO_4^{2-} compared to Cl^-. CEMs had a slightly higher selectivity towards potassium than sodium, i.e., ~1.2. SO_4^{2-} was strongly excluded from CEMs, most likely due to its double electric charge.

Moreover, EDBM performance indicators improved when multi-ions solutions were fed in the salt compartment. Current efficiency ranged from 70 % to 80 % at 1 mol L^{-1} OH^- target. At 0.5 mol L^{-1} and 1 mol L^{-1} targets, specific energy consumption in the range of 1.42–1.75 kWh kg^{-1}_{NaOH} and 1.60–1.94 kWh kg^{-1}_{NaOH} were obtained.

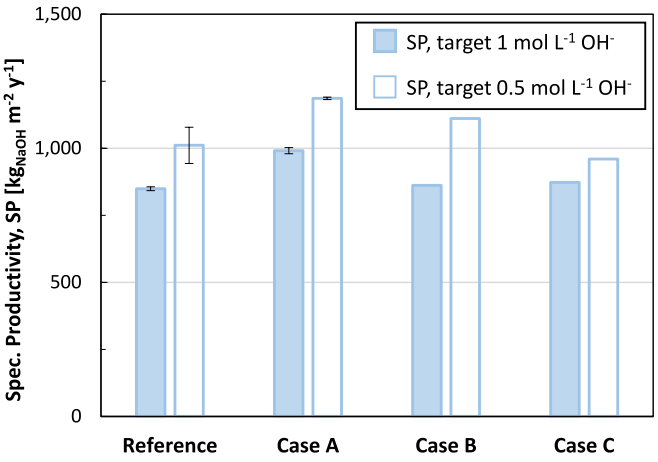

Fig. 9. Specific productivity referred to the kg of equivalent NaOH as function of investigated cases. Two targets of 0.5 mol L^{-1} OH– and 1 mol L^{-1} OH– were considered.

In addition to generating acids and bases, the EDBM can concentrate/dilute one ionic species relative to another, thus making the process interesting for the selective separation of ions.

Declaration of Competing Interest

The authors declare that they have no known competing financial interests or personal relationships that could have appeared to influence the work reported in this paper.

Data availability

The data will be shared at Zenodoo (https://zenodo.org/communities/searcularmine-project/?page=1&size=20)

Acknowledgements

This work was supported by the EU within SEArcularMINE (Circular Processing of Seawater Brines from Saltworks for Recovery of Valuable Raw Materials) project – Horizon 2020 programme, Grant Agreement No. 869467. This output reflects only the author's view. The European Health and Digital Executive Agency (HaDEA) and the European Commission cannot be held responsible for any use that may be made of the information contained therein.

The work of J. López was supported within the scope of Margarita Salas fellowship, financed by the Ministerio de Universidades (Spain) and European Union – NextGenerationEU.

Appendix A. Supplementary data

Supplementary data to this article can be found online at https://doi.org/10.1016/j.cej.2023.143673.

References

[1] J. López, O. Gibert, J.L. Cortina, Integration of membrane technologies to enhance the sustainability in the treatment of metal-containing acidic liquid wastes. An overview, Sep. Purif. Technol. 265 (2021), 118485, https://doi.org/10.1016/j.seppur.2021.118485.

[2] M. Bassyouni, M.H. Abdel-Aziz, M.S. Zoromba, S.M.S. Abdel-Hamid, E. Drioli, A review of polymeric nanocomposite membranes for water purification, J. Ind. Eng. Chem. 73 (2019) 19–46, https://doi.org/10.1016/j.jiec.2019.01.045.

[3] A. Campione, L. Gurreri, M. Ciofalo, G. Micale, A. Tamburini, A. Cipollina, Electrodialysis for water desalination: A critical assessment of recent developments

on process fundamentals, models and applications, Desalination 434 (2018) 121–160, https://doi.org/10.1016/j.desal.2017.12.044.
[4] J. Eke, A. Yusuf, A. Giwa, A. Sodiq, The global status of desalination: an assessment of current desalination technologies, plants and capacity, Desalination 495 (2020), 114633, https://doi.org/10.1016/j.desal.2020.114633.
[5] F.E. Ahmed, A. Khalil, N. Hilal, Emerging desalination technologies: current status, challenges and future trends, Desalination 517 (2021), 115183, https://doi.org/10.1016/j.desal.2021.115183.
[6] G.J. Doornbusch, M. Bel, M. Tedesco, J.W. Post, Z. Borneman, K. Nijmeijer, Effect of membrane area and membrane properties in multistage electrodialysis on seawater desalination performance, J. Memb. Sci. 611 (2020), 118303, https://doi.org/10.1016/j.memsci.2020.118303.
[7] M.M. Generous, N.A.A. Qasem, S.M. Zubair, The significance of modeling electrodialysis desalination using multi-component saline water, Desalination 496 (2020), 114347, https://doi.org/10.1016/j.desal.2020.114347.
[8] R.K. McGovern, S.M. Zubair, J.H. Lienhard V, The cost effectiveness of electrodialysis for diverse salinity applications, Desalination. 348 (2014) 57–65. https://doi.org/10.1016/j.desal.2014.06.010.
[9] A. Filingeri, M. Philibert, E. Filloux, N. Moe, A. Poli, A. Tamburini, A. Cipollina, Valorization of surface-water RO brines via Assisted-Reverse Electrodialysis for minerals recovery: performance analysis and scale-up perspectives, Desalination 541 (2022), 116036, https://doi.org/10.1016/j.desal.2022.116036.
[10] M. Philibert, A. Filingeri, C. Natalello, N. Moe, E. Filloux, A. Cipollina, Surface water RO permeate remineralization through minerals recovery from brines, Desalination 531 (2022), 115725, https://doi.org/10.1016/j.desal.2022.115725.
[11] L. Gurreri, M. la Cerva, J. Moreno, B. Goossens, A. Trunz, A. Tamburini, Coupling of electromembrane processes with reverse osmosis for seawater desalination: pilot plant demonstration and testing, Desalination 526 (2022), 115541, https://doi.org/10.1016/j.desal.2021.115541.
[12] V.V. Wagholikar, H. Zhuang, N.E. Moe, J. Barber, H. Ramanan, J.Y.H. Fuh, Analysis of RED/dRED stack performance using a resistances in series model, Desalination 496 (2020) 114505.
[13] X. Wang, Y. Wang, X. Zhang, H. Feng, T. Xu, In-situ combination of fermentation and electrodialysis with bipolar membranes for the production of lactic acid: continuous operation, Bioresour. Technol. 147 (2013) 442–448, https://doi.org/10.1016/j.biortech.2013.08.045.
[14] E. Rozoy, L. Boudesocque, L. Bazinet, Deacidification of cranberry juice by electrodialysis with bipolar membranes, J. Agric. Food Chem. 63 (2015) 642–651, https://doi.org/10.1021/jf502824f.
[15] Y. El Rayess, M. Mietton-Peuchot, Membrane technologies in wine industry: an overview, Crit. Rev. Food Sci. Nutr. 56 (2016) 2005–2020, https://doi.org/10.1080/10408398.2013.809566.
[16] A. Culcasi, L. Gurreri, A. Cipollina, A. Tamburini, G. Micale, A comprehensive multi-scale model for bipolar membrane electrodialysis (BMED), Chem. Eng. J. 437 (2022), 135317, https://doi.org/10.1016/j.cej.2022.135317.
[17] Y.u. Luo, Y. Liu, J. Shen, B. Van der Bruggen, Application of bipolar membrane electrodialysis in environmental protection and resource recovery: a review, Membranes (Basel). 12 (9) (2022) 829.
[18] R. Pärnamäe, S. Mareev, V. Nikonenko, S. Melnikov, N. Sheldeshov, V. Zabolotskii, H.V.M. Hamelers, M. Tedesco, Bipolar membranes: A review on principles, latest developments, and applications, J Memb Sci. 617 (2021), 118538, https://doi.org/10.1016/j.memsci.2020.118538.
[19] S.A. Mareev, E. Evdochenko, M. Wessling, O.A. Kozaderova, S.I. Niftaliev, N. D. Pismenskaya, V.v. Nikonenko, A comprehensive mathematical model of water splitting in bipolar membranes: Impact of the spatial distribution of fixed charges and catalyst at bipolar junction, J. Memb. Sci. 603 (2020), 118010, https://doi.org/10.1016/j.memsci.2020.118010.
[20] Y. Yang, X. Gao, A. Fan, L. Fu, C. Gao, An innovative beneficial reuse of seawater concentrate using bipolar membrane electrodialysis, J. Memb. Sci. 449 (2014) 119–126, https://doi.org/10.1016/j.memsci.2013.07.066.
[21] M. Reig, S. Casas, O. Gibert, C. Valderrama, J.L. Cortina, Integration of nanofiltration and bipolar electrodialysis for valorization of seawater desalination brines: Production of drinking and waste water treatment chemicals, Desalination 382 (2016) 13–20, https://doi.org/10.1016/j.desal.2015.12.013.
[22] A. Culcasi, R. Ktori, A. Pellegrino, M. Rodriguez-Pascual, M.C.M. van Loosdrecht, A. Tamburini, A. Cipollina, D. Xevgenos, G. Micale, Towards sustainable production of minerals and chemicals through seawater brine treatment using Eutectic freeze crystallization and Electrodialysis with bipolar membranes, J. Clean. Prod. 368 (2022) 133143.
[23] C. Cassaro, G. Virruso, A. Culcasi, A. Cipollina, A. Tamburini, G. Micale, Electrodialysis with bipolar Membranes for the sustainable production of chemicals from seawater brines at pilot plant scale, ACS Sustain. Chem. Eng. 11 (7) (2023) 2989–3000.
[24] SEArcularMINE, (n.d.). https://searcularmine.eu (accessed March 1, 2022).
[25] G. Battaglia, S. Romano, A. Raponi, D. Marchisio, M. Ciofalo, A. Tamburini, A. Cipollina, G. Micale, Analysis of particles size distributions in Mg(OH)2 precipitation from highly concentrated MgCl2 solutions, Powder Technol. 398 (2022), 117106, https://doi.org/10.1016/j.powtec.2021.117106.
[26] G. Battaglia, L. Berkemeyer, A. Cipollina, J.L. Cortina, M. Fernandez de Labastida, J. Lopez Rodriguez, D. Winter, Recovery of Lithium Carbonate from Dilute Li-Rich Brine via Homogenous and Heterogeneous Precipitation, Ind. Eng. Chem. Res. 61 (2022) 13589–13602, https://doi.org/10.1021/acs.iecr.2c01397.
[27] H.M. Saif, R.M. Huertas, S. Pawlowski, J.G. Crespo, S. Velizarov, Development of highly selective composite polymeric membranes for Li+/Mg2+ separation, J Memb Sci. 620 (2021), 118891, https://doi.org/10.1016/j.memsci.2020.118891.
[28] V. Vallès, J. López, M. Fernández de Labastida, O. Gibert, A. Leskinen, R. T. Koivula, J.L. Cortina, Polymeric and inorganic sorbents as a green option to recover critical raw materials at trace levels from sea saltwork bitterns, Green Chem. 25 (2) (2023) 700–719.
[29] F. Vicari, S. Randazzo, J. López, M. Fernández de Labastida, V. Vallès, G. Micale, A. Tamburini, G. D'Alì Staiti, J.L. Cortina, A. Cipollina, Mining minerals and critical raw materials from bittern: Understanding metal ions fate in saltwork ponds, Sci. Total Environ. 847 (2022), 157544, https://doi.org/10.1016/j.scitotenv.2022.157544.
[30] T. León, S. Abdullah Shah, J. López, A. Culcasi, L. Jofre, A. Cipollina, J.L. Cortina, A. Tamburini, G. Micale, Electrodialysis with Bipolar Membranes for the Generation of NaOH and HCl Solutions from Brines: An Inter-Laboratory Evaluation of Thin and Ultrathin Non-Woven Cloth-Based Ion-Exchange Membranes, Membranes (Basel). 12 (2022) 1204. https://doi.org/10.3390/membranes12121204.
[31] M. Herrero-Gonzalez, P. Diaz-Guridi, A. Dominguez-Ramos, A. Irabien, R. Ibañez, Highly concentrated HCl and NaOH from brines using electrodialysis with bipolar membranes, Sep. Purif. Technol. 242 (2020) 116785.
[32] B. Chen, C. Jiang, Y. Wang, R. Fu, Z. Liu, T. Xu, Selectrodialysis with bipolar membrane for the reclamation of concentrated brine from RO plant, Desalination 442 (2018) 8–15, https://doi.org/10.1016/j.desal.2018.04.031.
[33] C. Du, J.R. Du, X. Zhao, F. Cheng, M.E.A. Ali, X. Feng, Treatment of Brackish Water RO Brine via Bipolar Membrane Electrodialysis, Ind. Eng. Chem. Res. 60 (2021) 3115–3129, https://doi.org/10.1021/acs.iecr.1c00370.
[34] K. Song, S.-C. Chae, J.-H. Bang, Separation of sodium hydroxide from post-carbonation brines by bipolar membrane electrodialysis (BMED), Chem. Eng. J. 423 (2021) 130179.
[35] M. Wang, K.-K. Wang, Y.-X. Jia, Q.-C. Ren, The reclamation of brine generated from desalination process by bipolar membrane electrodialysis, J. Memb. Sci. 452 (2014) 54–61.
[36] K. Ghyselbrecht, A. Silva, B. van der Bruggen, K. Boussu, B. Meesschaert, L. Pinoy, Desalination feasibility study of an industrial NaCl stream by bipolar membrane electrodialysis, J. Environ. Manage. 140 (2014) 69–75, https://doi.org/10.1016/j.jenvman.2014.03.009.
[37] M. Reig, S. Casas, C. Valderrama, O. Gibert, J.L. Cortina, Integration of monopolar and bipolar electrodialysis for valorization of seawater reverse osmosis desalination brines: production of strong acid and base, Desalination 398 (2016) 87–97, https://doi.org/10.1016/j.desal.2016.07.024.
[38] W. Gao, Q. Fang, H. Yan, X. Wei, K. Wu, Recovery of acid and base from sodium sulfate containing lithium carbonate using bipolar membrane electrodialysis, Membranes (Basel). 11 (2021) 1–15, https://doi.org/10.3390/membranes11020152.
[39] A. Cournoyer, L. Bazinet, Electrodialysis processes an answer to industrial sustainability: toward the concept of eco-circular economy?—a review, Membranes (Basel). 13 (2) (2023) 205.
[40] C. Huang, T. Xu, Electrodialysis with bipolar membranes for sustainable development, Environ.. Sci. Technol. 40 (2006) 5233–5243, https://doi.org/10.1021/es060039p.
[41] Y. Zheng, R.J. MacDonald, Y.A. Ju, K.J. Sims, Bipolar Membrane and Method of Making Same, US 2006/0173084 A1, 2006.
[42] SUEZ, Ionics* Ion Exchange Membranes. Water Technologies & Solutions. Fact Sheet, (n.d.). https://www.watertechnologies.com/products/ionics-ion-exchange-membranes (accessed October 12, 2022).
[43] A. Culcasi, L. Gurreri, A. Tamburini, I.D. Lockhart Bogle, G. Micale, A bi-objective optimization study of an acid-base flow battery for high efficiency and improved power density, Chem. Eng. Trans. 96 (2022) 133–138, https://doi.org/10.3303/CET2296023.
[44] H. Strathmann, J.J. Krol, H.-J. Rapp, G. Eigenberger, Limiting current density and water dissociation in bipolar membranes, J Memb Sci. 125 (1997) 123–142, https://doi.org/10.1016/S0376-7388(96)00185-8.
[45] U.S. Geological Survey, PHREEQC Version 3, (2017). https://www.usgs.gov/software/phreeqc-version-3.
[46] P. Vanýsek, Ionic conductivity and diffusion at infinite dilution, CRC Handbook of Chemistry and Physics. 96 (1996) 5–98.
[47] Y. Marcus, Ionic radii in aqueous solutions, Chem. Rev. 88 (1988) 1475–1498, https://doi.org/10.1021/cr00090a003.